Journal of Applied Polymer Science

WILEY

Applied Polymer SCIENCE

RESEARCH ARTICLE

Enhancing Odor Reduction and Properties in Polypropylene-Based Wood Plastic Composites With Halloysite Nanotubes and Beta-Cyclodextrin

Gizem Kurtulmus[1,2,3] | Yusuf Ziya Menceloglu[1,2]

[1]Faculty of Engineering and Natural Sciences, Material Science and Nano Engineering, Istanbul, Turkey | [2]Sabanci University Integrated Manufacturing Technologies Research and Application Center & Composite Technologies Center of Excellence, Istanbul, Turkey | [3]Kastamonu Integrated Wood Industry Co. Inc., R&D Center, Istanbul, Turkey

Correspondence: Yusuf Ziya Menceloglu (yusufm@sabanciuniv.edu)

Received: 28 April 2025 | **Revised:** 4 July 2025 | **Accepted:** 11 July 2025

Funding: This work was supported by the Turkish Scientific and Technological Research Council of Türkiye (TÜBİTAK) and Kastamonu Entegre Wood Industry Co. Inc. incorporated company with Project Numbers 118C042 and 5230043.

Keywords: adsorption | composites | nanoparticles, nanowires and nanocrystals | nanotubes, graphene and fullerenes | thermoplastics

ABSTRACT

Undesirable odor emissions that originate from polypropylene (PP)-based wood plastic composites (WPCs) caused by volatile organic compounds (VOCs) restrict their indoor applications. This research investigates the effectiveness of halloysite nanotubes (HNT) and beta-cyclodextrin (β-CD) in reducing VOC emissions while simultaneously improving the mechanical and thermal properties of WPCs. Composites are produced by incorporating 2 wt.% and 5 wt.% of HNT, β-CD and are compared to commercial odor-control additives. Odor intensity is tested using sensory (jar) odor and headspace gas chromatography–mass spectrometry (HS GC–MS) methods. Mechanical, thermal, morphological, and structural properties are characterized through tensile testing, thermogravimetric analysis (TGA), differential scanning calorimetry (DSC), scanning electron microscopy (SEM), Fourier-transform infrared spectroscopy (FTIR), and Brunauer–Emmett–Teller (BET) analysis. The odor results show the addition of 5 wt.% HNT and 2 wt.% β-CD causes a reduction of VOC peaks by 14% and 35%, respectively. HNT results in a 36.6% reduction of 4-methyl-octane and improves tensile strength and modulus by 6.3 (±0.3) % and 12 (±0.8) %, whereas β-CD advances in toughness. The BET and FTIR analyses confirm distinct adsorption behaviors and interactions within the polypropylene matrix. These results suggest the potential of HNT and β-CD as sustainable additives to improve the indoor applicability of PP-based WPCs.

1 | Introduction

In light of increasing environmental challenges related to population growth, governments globally have implemented regulations with the purpose of creating the evolution towards a circular economy. These regulations point out the importance of resource efficiency and the necessity of reducing plastic waste. In this framework, the European Green Deal outlines the necessity for integrating renewable materials into plastic-based products, directing a minimum of 25% by 2025 and 55% by 2030. The plan intends to decrease dependence on fossil-based resources and lower impacts on the environment [1]. In a parallel manner, the United States Environmental Protection Agency (EPA) aims for a 50% renewable content in plastic production [2]. Within this statutes and regulations, wood plastic composites (WPCs), which combine natural fibers such as wood flour with thermoplastics like polypropylene (PP), have gained considerable attention as sustainable material alternatives.

[Correction added on August 19, 2025, after first online publication: The copyright line was changed.]

Wood-plastic composites (WPCs) are usually produced with polyethylene, and wood fibers have been used for outdoor applications. Conversely, WPCs that consist of polypropylene provide increased mechanical and thermal properties, offering them suitability for indoor applications such as automotive components and consumer products [3]. Polypropylene is widely used because of its cost-effectiveness, resistance to moisture, and beneficial chemical stability [4]. Even so, we want to use the recycled polypropylene; it presents a substantial challenge regarding odor emissions, especially in indoor environments. The odors observed are mainly caused by volatile organic compounds (VOCs) emitted during the thermal degradation of polypropylene during production and the decomposition of residual additives and contaminants [5–7].

The addition of wood fibers to polypropylene further raises odor emissions. Volatile organic compounds (VOCs) originated from wood, which includes formaldehyde, acetaldehyde, and acetic acid, are released during processing, with elevated temperatures intensifying this problem [8–10]. These emissions in disputes adversely influence the acceptability and environmental performance of wood-plastic composites aimed at indoor applications. Thus, the reduction of VOC emissions is essential for improving both the functionality of materials and the acceptance by users.

Despite process-level treatments, involving degassing and adjustments of molding parameters, having been looked into for odor elimination, material-based solutions have shown more effective results [11–13]. They are the additives, such as zeolites, copper-coated silica, activated carbon, and carbon nanotubes, that have been examined for their capacity to adsorb volatile organic compounds (VOCs) [14, 15]. Among these materials, halloysite nanotubes (HNTs) and β-cyclodextrin (β-CD) have emerged as notably promising candidates, attributed to their distinctive chemical structures and adsorption properties.

β-cyclodextrin is a cyclic oligosaccharide that is formed from seven glucose units. The toroidal molecular structure features a hydrophobic cavity and a hydrophilic outer surface, enabling the formation of stable inclusion complexes with hydrophobic volatile organic compounds, including aromatic hydrocarbons [16, 17]. Halloysite nanotubes are naturally occurring aluminosilicate minerals that are characterized by their hollow tubular structures. Their high surface area, dual surface charge, and large aspect ratio characteristics lead to their efficacy as nanofillers and potential adsorbents for VOCs within polymer matrices [18–20].

A comparative analysis of HNTs and β-CD with other materials reveals significant advantages in terms of performance, safety, and environmental impact. Zeolites, while effective in adsorbing VOCs, are more expensive and mechanically weaker than HNTs, which possess a robust nanoscale tubular structure [21, 22]. β-CD, known for its hydrophilic nature, is also effective in VOC adsorption and offers advantages such as chemical stability and aqueous solubility. The odor-removal efficiency of copper-coated silica varies with copper loading, while both HNTs and β-CD provide consistent results. HNTs can be converted into carbon nanoflakes for enhanced CO_2 adsorption and supercapacitance, offering a non-toxic alternative to carbon nanotubes (CNTs) [23, 24]. In polymer composites, HNTs have been shown to improve impact resistance more effectively than CNTs, which tend to be brittle [25]. While graphene offers superior mechanical reinforcement, HNTs and β-CD are more cost-effective and biocompatible. Biochar may interfere with biological systems, whereas β-CD is widely regarded as safe and effective in various applications, including environmental and pharmaceutical uses [26, 27].

Even though HNTs and β-CD represent particular potential for the adsorption of VOCs, their specific usage for decreasing odor emissions in polypropylene-based wood-plastic composites (WPCs) remains not properly explored. While β-CD has established its effectiveness in the adsorption of VOCs such as formaldehyde and xylene, and halloysite nanotubes (HNTs) have been highlighted for their ability to improve mechanical strength, there exists an absence of research investigating their individual effects within composite systems intended for odor control by reducing odorous VOCs [28–30].

This study investigates the individual effects caused by HNT and β-CD on the VOC emissions, mechanical, and other characteristics of polypropylene-based WPCs for addressing this gap. The research proposes to obtain a dual benefits by reducing odor levels and improving the physical performance of WPCs. The uniqueness of this study lies in its comprehensive material approach, which promotes the development of sustainable, functional composites in line with the requirements of the circular economy.

2 | Materials and Methodology

2.1 | Materials

Polypropylene (PP) HE125MO homopolymer that has a density of 905 kg/m^3, melt flow rate (MFR) value 12 g/10 min (230°C/2.16 kg), and derived in white granule form for injection molding application were supplied by Borealis Compounds Inc., North Carolina, USA. Wood Fiber with 20-40 micrometer (μm) width 1.5–2.5 mm weighted average length and consists of 70 wt.% oak (*Quercus robur*) and 30 wt.% pine (*Pinus sylvestris*) is supplied by Kastamonu Integrated Wood Industry Co Inc., Gebze/Kocaeli, Türkiye. Halloysite nanotube (HNT) was obtained from Esan Eczacıbaşı Industrial Raw Materials Industry and Trade Inc., Maltepe, Türkiye. STRUKTOL RP 53 odor control additive (mask) has an off-white pastille form for compounding PE and PP WPC products provided by Struktol Company of America LLC, Ohio, US. TEGO Sorb PY88TQ is a zinc ricinoleate containing 8.8%–10.8% zinc, used as odor absorber in form of pale-yellow pellets. It is used for the production of masterbatches and compounds that are suitable for Polyolefins were supplied by Evonik Nutrition & Care GmbH, Essen, Germany. β-Cyclodextrin ≥97% purity in white powder form with was purchased from Sigma Aldrich, Merck Group, St. Louis, Missouri, USA.

2.2 | Preparation of PP Based WPC Formulations

Wood fiber (WF) and polypropylene (PP) were dried at 80°C for 24 h prior to the preparation of wood-plastic composite (WPC)

TABLE 1 | Table of indoor odor (jar) test results.

Sample name	Test condition	Rating average	Result
70PP-30WF	1 (25°C, 24 h)	3.0	Very perceptible but not disturbing
	2 (40°C, 24 h)	3.5	Intense enough to be slightly disturbing
	3 (65°C, 2 h)	4.0	Disturbing
68PP-30WF-2HNT	1 (25°C, 24 h)	2.5	Clearly perceptible but not disturbing
	2 (40°C, 24 h)	3.0	Very perceptible but not disturbing
	3 (65°C, 2 h)	3.5	Intense enough to be slightly disturbing
65PP-30WF-5HNT	1 (25°C, 24 h)	1.5	Slightly perceptible
	2 (40°C, 24 h)	2.0	Perceptible, not disturbing
	3 (65°C, 2 h)	2.5	Clearly perceptible but not disturbing
68PP-30WF-2β-CD	1 (25°C, 24 h)	1.5	Slightly perceptible
	2 (40°C, 24 h)	2.0	Perceptible, not disturbing
	3 (65°C, 2 h)	2.5	Clearly perceptible but not disturbing
65P-30WF-5β-CD	1 (25°C, 24 h)	2.0	Perceptible, not disturbing
	2 (40°C, 24 h)	2.5	Clearly perceptible but not disturbing
	3 (65°C, 2 h)	3.0	Very perceptible but not disturbing
68PP-30WF-2RP53	1 (25°C, 24 h)	2.5	Clearly perceptible but not disturbing
	2 (40°C, 24 h)	3.0	Very perceptible but not disturbing
	3 (65°C, 2 h)	3.5	Intense enough to be slightly disturbing
68PP-30WF-2PY88TQ	1 (25°C, 24 h)	3.0	Very perceptible but not disturbing
	2 (40°C, 24 h)	3.5	Intense enough to be slightly disturbing
	3 (65°C, 2 h)	4.0	Disturbing

formulations. The base composition consisted of 70 wt.% PP and 30 wt.% WF, with additives incorporated at varying concentrations: 2 wt.% and 5 wt.% Halloysite Nanotubes (HNT), 2 wt.% and 5 wt.% β-Cyclodextrin (β-CD), and 2 wt.% STRUKTOL RP 53 and TEGO Sorb PY 88 TQ. The formulations were processed using a Gelimat GI ultra-high-speed thermokinetic mixer (Draiswerke, USA), which is characterized by high shear forces and short retention times. During mixing, the components were compounded at approximately 4000 rpm, resulting in a chamber temperature of 180°C. After mixing, the wood-plastic composite was subjected to cooling and granulation using a plastic granulator (Rhong Machinery, China). The granules were subsequently transformed into specimens suitable for mechanical and thermal evaluation through injection molding (Xplore, Sittard, Holland) at a melt temperature of 240°C, a mold temperature of 35°C, and an injection pressure of 12 bar.

2.3 | Characterization

The Jar (odor) test was conducted to evaluate the odor intensity of wood–plastic composites (WPCs) formulated with 70 wt.% polypropylene (PP) and 30 wt.% wood flour (WF). The sample set included: (i) a control WPC without additives, (ii) WPCs modified with 2 wt.% and 5 wt.% halloysite nanotubes (HNT), (iii) WPCs containing 2 wt.% and 5 wt.% β-CD, and WPCs incorporating 2 wt.% of commercial odor-control additives RP 53 and PY88TQ. As part of the pre-conditioning, all specimens were exposed to ambient laboratory conditions (approximately 23°C and 50% relative humidity) for a duration of 12 days to simulate environmental aging. Subsequently, the samples were individually placed in 1 L gas-tight glass jars containing 50 mL of distilled water at the base. A stainless-steel wire mesh was positioned above the water to suspend the samples and prevent direct contact. Following sample preparation, all specimens were subjected to three different temperature conditions to simulate various storage and handling scenarios: (i) 25°C for 24 h, (ii) 40°C for 24 h, and (iii) 65°C for 2 h. After exposure, the odor intensity of each sample was evaluated by a panel of five independent raters. To ensure objective evaluation, the jars were anonymized and randomly labeled from 1 to 7, with no reference to their contents. Odor intensity was rated on a scale from 1 to 6 (1 = imperceptible odor, 6 = Extremely disturbing odor). The average ratings from the panelists are presented in Table 1.

Headspace Gas Chromatography-Mass Spectrometry (HS GC-MS) analyzed for identification of VOCs of samples. Extraction of VOCs was performed using 1 g sample in a 10 mL HS-vial with a PTFE septum. The samples were conditioned and

equilibrated at 125°C with agitation at 250 rpm for headspace enrichment. A HS-20NX Headspace Autosampler (Shimadzu Scientific Instruments, USA) was used for automated sampling. The injection was performed at 200°C with an injection time of 5 s and a split ratio of 1:20. The analysis was carried out on a GC-MS-QP2010 Ultra system (Shimadzu Scientific Instruments, Carlsbad, CA, USA) equipped with an InertCap Pure-WAX capillary column (60 m × 0.25 mm × 0.25 μm film thickness). Helium was used as a carrier gas at a constant flow rate of 1 mL/min and an average linear velocity of 22 cm/s.

The GC oven was programmed to heat from 50°C to 200°C using a multi-rate temperature gradient: 3°C/min from 50°C to 100°C, followed by 12°C/min to 200°C. The total running time for each analysis was 30 min. The injector temperature was set to 250°C, and the MS detector was operated in scan mode within a mass range of 30–550 m/z. Blank runs were conducted between samples to prevent cross- contamination.

Identification of VOCs was based on retention times and mass spectra comparison with reference spectra from the WILEY7/NIST mass spectral libraries. For quantification, a seven-point calibration curve was constructed using acetone as the internal standard in 1-butanol at concentrations of 0.1, 0.5, 1, 5, 10, 50, and 100 grams per liter (g/L). A 5 microliter (μL) syringe was used to inject 2 μL of each calibration solution into 10 mL HS vials under identical conditions. The limit of detection (LOD) for VOCs was defined as peaks with heights at least three times the baseline noise and areas exceeding 10% of the acetone peak area at a concentration of 0.5 g/L acetone.

Tensile properties of the polypropylene (PP)-based wood–plastic composites (WPCs) were evaluated in accordance with the ISO 527-2 standard using a universal testing machine (Instron 100 kilonewton (kN) Electromechanical Test System, Massachusetts, USA). A total of five replicates ($n = 5$) of Type 1A dog-bone specimens, each with a thickness of 2 mm and width of 5 mm in the gauge section, were tested. The experiments were conducted using a 5 kN load cell at a constant crosshead speed of 100 mm/min. An extensometer was employed to accurately record the strain and calculate the percentage elongation at break. This setup enabled the precise determination of tensile strength, modulus of elasticity, and elongation behavior of the composite materials.

The surface morphologies of samples were characterized using Field Emission Scanning Electron Microscopy (FESEM, CARL ZEISS LEO SUPRA 35VP) operated at an accelerating voltage of 5 kV in secondary electron (SE) mode. Micrographs were acquired at a magnification of 10 K X to observe the microstructural features in detail. Fracture surfaces were obtained by mechanically breaking the specimens at room temperature, and imaging was conducted on the fractured cross-sections to evaluate the interfacial adhesion and dispersion of components. Prior to imaging, the sample surfaces were sputter-coated with carbon in three layers to ensure adequate electrical conductivity and minimize charging effects during analysis.

Fourier-transform infrared (FTIR) spectroscopy analysis of the composites was conducted using a Thermo Scientific Nicolet iS10 FTIR spectrometer (Waltham, Massachusetts, USA), equipped with a diamond Attenuated Total Reflection (ATR) crystal. FTIR spectra were recorded using OMNIC 9.2.98 software (Thermo Fisher Scientific, Gloucester, UK), within the wavelength range of 4000–600 cm^{-1} and a resolution of 4 cm^{-1}. The analysis was performed to identify the presence of functional groups and to investigate interactions among the various components of the composites. A total of 32 scans were collected to enhance the signal-to-noise ratio.

The thermal stability of the specimens was assessed using thermogravimetric analysis (TGA) conducted on a Mettler Toledo instrument (Giessen, Germany). Alumina crucibles with a volume of 90 μL were utilized for the analysis. Each mass of the samples was approximately 11–12 mg. TGA thermograms were acquired using STAR SW 16.10 software (Mettler Toledo, Columbus, OH, USA). The tests were performed under a nitrogen atmosphere, spanning a temperature range of 20°C to 700°C, with a heating rate of 10°C/min.

The effect of HNT, β-CD, and other additives on the thermal transition temperatures and crystallinity of the PP polymer was analyzed under an inert nitrogen atmosphere with a Differential Scanning Calorimeter (DSC) (Mettler Toledo DSC 3, Giessen, Germany). 100 μL aluminum crucibles were used for testing. The weight of each sample was approximately 10–11 mg. STAR SW 16.10 software (Mettler Toledo, Columbus, OH, USA) was used to determine the melting enthalpy (ΔHm), melting temperature (Tm), cold crystallization temperature (Tc), and cold crystallization enthalpy (ΔHc). DSC analysis was performed in three cycles. In the first step of the cycle, the samples were heated from room temperature to 200°C at 10°C/min and held at 200°C for 2 min to erase their thermal history. In the second cycle, the samples were cooled from 200°C to −70°C at a rate of 10°C/min and held at −70°C for 2 min. The cold crystallization temperatures (Tc) were determined from the maximum points of the peaks in the resulting thermogram. In the third cycle, the samples were reheated from −70°C to 200°C at a rate of 10°C/min, and the melting temperatures (Tm) were derived from the peak maxima observed during this final heating. The degree of crystallinity (Xc) for each sample was calculated using (Equation (1)):

$$X_c = \left[\Delta H_m / \Delta H_m^{\circ} \times \left(100 - w^F\right)\right] \times 100\% \quad (1)$$

where ΔH_m is the melting enthalpy and ΔH_m° is the melting enthalpy of 100% crystalline polymer and w^F corresponds to the weight percentage of fiber in the composite. The theoretical value of 100% crystalline polypropylene (ΔH_m°) is 207 J/g [31, 32].

The surface area and porosity of HNT and β-CD were measured using nitrogen adsorption–desorption at 77 K with the Brunauer–Emmett–Teller (BET) and Barrett–Joyner–Halenda (BJH) methods, employing a high-performance gas adsorption analyzer (Micromeritics 3Flex, Norcross, GA, USA). The specific surface areas of the samples were determined using the BET technique, while the pore size and pore volume were calculated from the desorption isotherm curves using the BJH method and the maximum amount of nitrogen adsorbed at a relative pressure of $P/P_0 = 0.99$. The degassing pressure during the outgassing process reached 1.0 mmHg. All samples were subjected to vacuum outgassing at 80°C for 24 h prior to measurement.

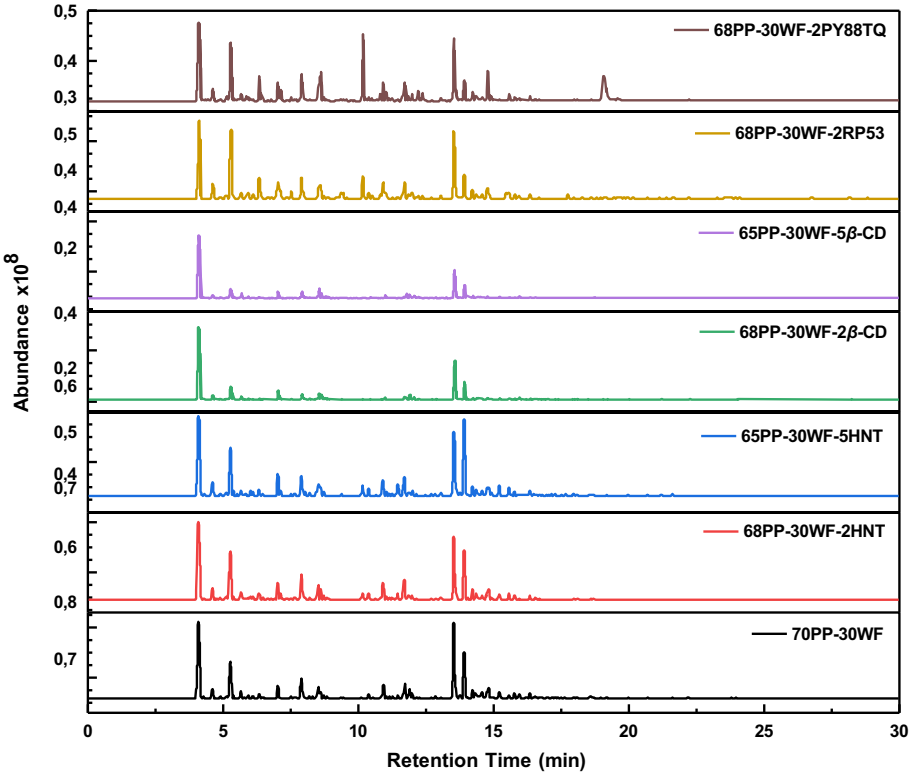

FIGURE 1 | HS GC–MS chromatograms of 30 wt.% WF and 70 wt.% PP based WPC, 2 and 5 wt.% HNT, β-CD, 2 wt.% RP53, and PY88TQ added WPCs. [Color figure can be viewed at wileyonlinelibrary.com]

3 | Results and Discussion

3.1 | Sensory Analysis Result

The odor effect of HNT, β-CD, and commercial additives (RP53 and PY88TQ) on WPCs has been investigated by Indoor Odor (Jar) test (FORD FLTM BO 131–03 Interior Odor Test standard). The outcomes were presented in Table 1. Based on that table, the odor reached a "disturbing" level when WPC is formed with the addition of wood fiber and PP. Additionally, the odor level of WPC reduced from 4 (disturbing) to 3 (intense enough to be slightly disturbing) with 2 wt.% HNT. An increase in concentration to 5 wt.% HNT led to a higher reduction in odor levels relative to the 2 wt.% HNT, which lowered the rating from 4 (disturbing) to 2.5 (not disturbing). This effect is attributable to HNT's unique porous tubular morphology and surface characteristics, which allow for effective VOC adsorption [33]. In addition, this result was affected by the high surface area and VOC adsorption ability of HNT due to being a nanoparticle.

Furthermore, increasing the concentration from 2 to 5 wt.% improved the adsorption capacity of HNT. A similar outcome with the 5 wt.% HNT containing WPC was also achieved by adding 2 wt.% β-CD that has adsorption ability due to its porous structure. However, increasing the β-CD concentration to 5 wt.% did not yield additional odor reduction, unlike HNT. Considering this, the adsorption capacity of β-CD for odor- forming VOCs in WPC was exceeded at this concentration. These results are attributed to the porous structure and high surface area of HNT, which physically adsorbs VOCs, and the host–guest complexation capability of β-CD [5, 34]. Due to the subjective nature of the aforementioned test, it was determined that another supportive and more qualitative test methods were needed such as HS GC-MS.

Analytical techniques have been developed to identify VOC emissions and related odors in plastics and their composite materials. Olfactometry is frequently used to detect and measure the odors produced by VOCs. Samples with intense odors may indicate higher concentrations of VOCs, while mild odors may suggest lower VOC levels. The assessment of odor type and intensity is typically subjective; therefore, involving multiple evaluators help ensure a more accurate evaluation [8]. VOCs released from plastics, including Polypropylene (PP), can also be identified using Gas Chromatography (GC) combined with either a Flame Ionization Detector (FID) or Mass Spectrometry (MS), providing more objective results than olfactometry. GC/MS, especially when used with the headspace (HS) technique, allows VOCs to disperse into the gas phase from a solid matrix, offering more accurate and reliable results. Detailed odor characterization often requires a combination of instrumental and sensory analysis techniques [35–37]. Therefore, in this study, HS GC–MS and olfactory methods were applied to investigate VOCs responsible for the unpleasant odors of PP-based WPCs.

3.2 | Characterization of VOCs by HS GC–MS Result

HS GC–MS chromatogram of the volatile compounds from 30 wt.% WF and 70 wt.% PP-based WPC, 2 and 5 wt.% HNT, β-CD, and 2 wt.% RP53, PY88TQ added WPCs are shown in

TABLE 2 | Undesirable odor VOCs identified according to the HS GC–MS chromatogram.

Sample name	Total VOC peaks numbers[a]	Reduction rate (%)	Height decreased VOCs	Height decreasing rate [%]
70PP-30WF	28	—	—	—
70PP-30WF-2HNT	24	14	Octane 4-methyl-/Acetic acid/Ammonium Oxalate	1.4/17.3/6.1
70PP-30WF-5HNT	24	14	Octane, 4-methyl-/Dodecane, 4,6-dimethyl–/Nonane, 5-butyl/Acetic acid/1-Octanol	36.6/10.3/46.4/3.2/23.3
68PP-30WF-2β-CD	18	35	Octane, 4-methyl-/Heneicosane, 11-(1-ethylpropyl)-/2-Furancarboxaldehyde/ Benzaldehyde	9.4/43.0/21.8/36.3
65PP-30WF-5β-CD	18	35	Octane, 4-methyl-/Heneicosane, 11-(1-ethylpropyl)-/2-Furancarboxaldehyde/ Benzaldehyde	9.4/43.0/21.8/36.3
68PP-30WF-2RP53	17	39	Acetic acid/2-Furancarboxaldehyde (Furfural)	9.4/48.5
70PP-30WF-2PY88TQ	23	17	Acetic acid/2-Furancarboxaldehyde (Furfural)	15.6/55.3

[a]After reducing peaks according to 10% Acetone (control and calibration solution) peak height.

Figure 1. The main peaks of the WPC spectrums are nearly identical to those of other WPCs, indicating that these represent the primary constituent materials. However, there were distinct peaks in Table 2 that could not be attributed to PP or wood materials in WPC. These volatile compounds may result from residual impurities in the raw materials or degradation during processing. Dodecanoic acid (CAS) lauric acid shows up at the 19th min in samples found in 2 wt.% PY88TQ added WPCs as in Figure 1.

In the analysis, 48 VOCs were identified in PP-based WPC via a reference database matching VOCs by their mass spectra and retention times. By the elimination of peaks lower than 10% of acetone peak height, the number of VOCs decreased to 28 in WPC without additive, 24 with HNT, 23 with PY88TQ, and 18 with β-CD, as presented in Table 2. The additives reduced VOC peaks by 14%, 17%, and 35%, respectively. HNT was especially effective in lowering the levels of VOCs, such as octane 4-methyl, acetic acid, and nonane 5-butyl. Among these, nonane 5-butyl and octane 4-methyl were reduced mostly. Additionally, 2,4-Dimethyl-heptane, a compound linked to the pungent plastic odor [9], disappeared completely when additives like HNT, PY88TQ, or β-CD were used. HNT had the biggest impact, reducing 4-methyl-octane—a main odor-causing VOC—by 37%, likely due to its ability to bind VOC molecules through intermolecular interactions. HNT was also quite efficient in reducing acetic acid VOCs, which are produced by wood fibers in WPC.

Compared to PY88TQ, HNT was more feasible at minimizing acetic acid caused by both the wood fibers and the PP in the composite [8, 38]. Moreover, PY88TQ, at a 2 wt.% concentration, was more useful than RP53 and β-CD in reducing 2-furancarboxaldehyde (Furfural), a VOC formed during the breakdown of hemicellulose in wood fibers [39]. β-CD, on the other hand, was particularly good at reducing peaks of heneicosane 11-(1-ethylpropyl)- and benzaldehyde. These trends align with previous studies showing that HNT can non-selectively adsorb hydrocarbons, while β-CD selectively captures polar VOCs via its hydrophobic cavity [40, 41].

3.3 | Mechanical Test Result

Figure 2 shows the stress–strain curves of all samples as a result of the tensile test. Their data regarding the test analyses are given in Table 3.

The results indicated that the tensile modulus of PP was increased by 63% by adding 30 wt.% WF. From analysis of the additives on the modulus of WPCs, it can be seen that the tensile modulus increased proportionally with the content of HNT, and the most noticeable increase was observed in the WPC containing 5 wt.% HNT. The enhancement is due to the restriction of movement at molecular chains PP by HNT hence giving more resistance to deformation for the material. The modulus values of WPCs containing 30 wt.% wood fiber were approximately increased by 8 (±0.7) %, 12 (±0.8) %, 3 (±0.8), % and 10 (±0.7) % after the addition of 2 wt.% and 5 wt.% HNT. 2 wt.% RP53, and 2 wt.% PY88TQ, respectively. However, the addition β-CD at concentrations of 2 wt.% and 5 wt.% resulted in a reduction in the modulus of 13 (±0.09) % and 3 (±0.8) %, respectively. This decrease can be explained by the weak binding interactions that exist between the PP polymer and β-CD. During the procedure, the complexing agent may be

reduced due to hydrophobic, inactive, and non-adhering polymer. Tensile strength followed a similar trend to tensile modulus for HNT containing WPCs. So, integrating 2 wt.% HNT and 5 wt.% HNT to WPC increased the tensile strength by 4.5 (±0.6) % and 6.3 (±0.3) %, respectively. This can be attributed to improved fiber-matrix interaction, as confirmed by FESEM imaging. HNT likely acts as a rigid filler and nucleating agent, contributing to the stiffness and load-bearing capacity of the composite [42].

The tensile strength of 2 wt.% and 5 wt.% β-CD including WPCs slightly increased 1.7 (±0.7) % and 0.6 (±0.4) %, respectively. Conversely, 2 wt.% β-CD provided the highest strain at break (4.3%), suggesting improved toughness. The reduction in elongation in HNT-reinforced WPCs can be explained by the fact that the increasing HNT content, particularly at 5 wt.%, restricts the movement of polymer chains, preventing them from aligning in the direction of tension. Additionally, HNT aggregation in the PP matrix creates stress concentration points, leading to premature fractures [43].

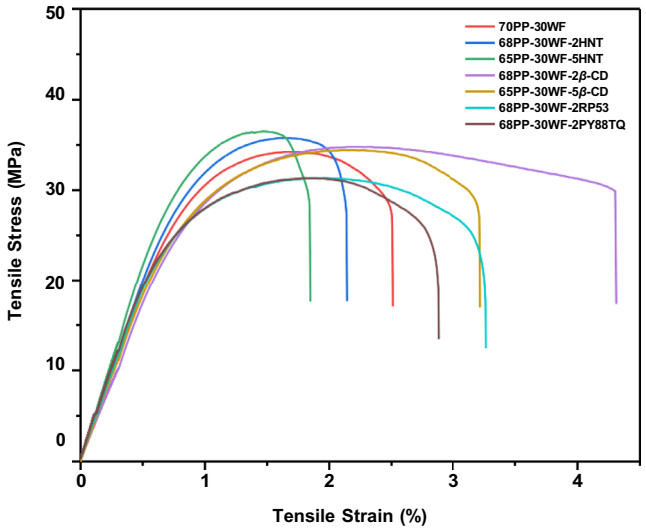

FIGURE 2 | Stress–strain graph of the 30 wt.% WF containing WPC and formulations with the additives. [Color figure can be viewed at wileyonlinelibrary.com]

3.4 | Morphological Analysis

Figure 4 presents FESEM micrographs obtained from the cross-sectional fracture surfaces of specimens broken during tensile testing. Neat polypropylene (PP), was imaged as the control for comparison, as shown in Figure 3a, was imaged as the control for comparison and exhibits a smooth and relatively featureless surface with occasional voids and fiber-like elongations. This morphology is typical of ductile polymers and supports its baseline mechanical behavior, particularly lower stiffness, and higher strain at break. Figure 3b demonstrates that the addition of 30 wt.% WF results in a less smooth surface and more brittle, fractured fibrous ends. Furthermore, debonding, fiber pull-out, and voids left by broken fibers indicate a distinct interface between the PP matrix and the wood fibers. The weak interfacial bonding between the hydrophilic WF and the hydrophobic PP matrix is a phenomenon also widely documented in natural fiber composites [44]. At low HNT content, the FESEM images (Figure 3c,d) show homogeneously dispersed nanoparticles and reduced voids, confirming improved interfacial adhesion and stress transfer. These morphological improvements are mirrored in tensile strength as well. [42]. HNT nanoparticles that have particle sizes under 200 nm within the PP matrix as seen in Figure 3c. The same chromatogram also includes the effect of fibrous structure of PP. Figure 3d illustrates that increasing the HNT content from 2 wt.% to 5 wt.% results in a rougher surface morphology. In the composite containing 2 wt.% HNT, distinct holes are observed, whereas in the 5 wt.% HNT sample, these are replaced by shallower surface cavities. This change suggests improved dispersion and interaction of HNTs within the matrix at higher loading levels, which is consistent with findings reported in similar polymer nanocomposite systems [45]. Additionally, while thicker wood fibers generally exhibit reduced interfacial adhesion with the polypropylene (PP) matrix, thinner wood fiber enhance matrix-fiber interaction due to their larger specific surface area and improved wettability [46]. This improved adhesion, combined with the increased HNT content, contributes to the best reinforcing effect observed in the WPC formulation containing 5 wt.% HNT. As demonstrated in Figure 3e, WPC with the commercial additive RP53 has micro-fractured fibrous ends on the matrix surface. In the WPC prepared with PY88TQ, due to the insufficient bond between the fiber and the matrix, the voids caused by the particles that migrated on the matrix surface and the gap between the fiber were

TABLE 3 | Table of tensile test results of the samples.

Sample name	Tensile strength [MPa]	Tensile modulus [MPa]	Tensile strain at break [%]	Elongation at break [MPa]	Yield stress [MPa]
70PP-30WF	34.2 (±0.3)[a]	3971.1 (±53.7)	2.5 (±0.1)	28.3 (±0.7)	34.2 (±0.3)
70PP-30WF-2HNT	35.8 (±0.7)	4312.6 (±207.8)	2.1 (±0.1)	29.9 (±1.1)	35.8 (±0.7)
65PP-30WF-5HNT	36.5 (±0.4)	4504.5 (±228.9)	1.8 (±0.1)	29.9 (±2.5)	36.5 (±0.4)
68PP-30WF-2β-CD	34.8 (±0.9)	3458.7 (±58.9)	4.3 (±1.4)	30.0 (±13.7)	34.8 (±0.9)
65PP-30WF-5β-CD	34.4 (±0.5)	3866.1 (±260.2)	3.2 (±1.2)	28.3 (±12.1)	34.4 (±0.5)
68PP-30WF-2RP53	31.3 (±1.0)	4097.8 (±292.7)	3.2 (±0.7)	21.5 (±7.5)	31.3 (±1.0)
68PP-30WF-2PY88TQ	31.3 (±0.9)	4403.1 (±183.3)	2.9 (±0.6)	22.4 (±10.1)	31.3 (±0.9)

[a]Values in parentheses are standard deviations.

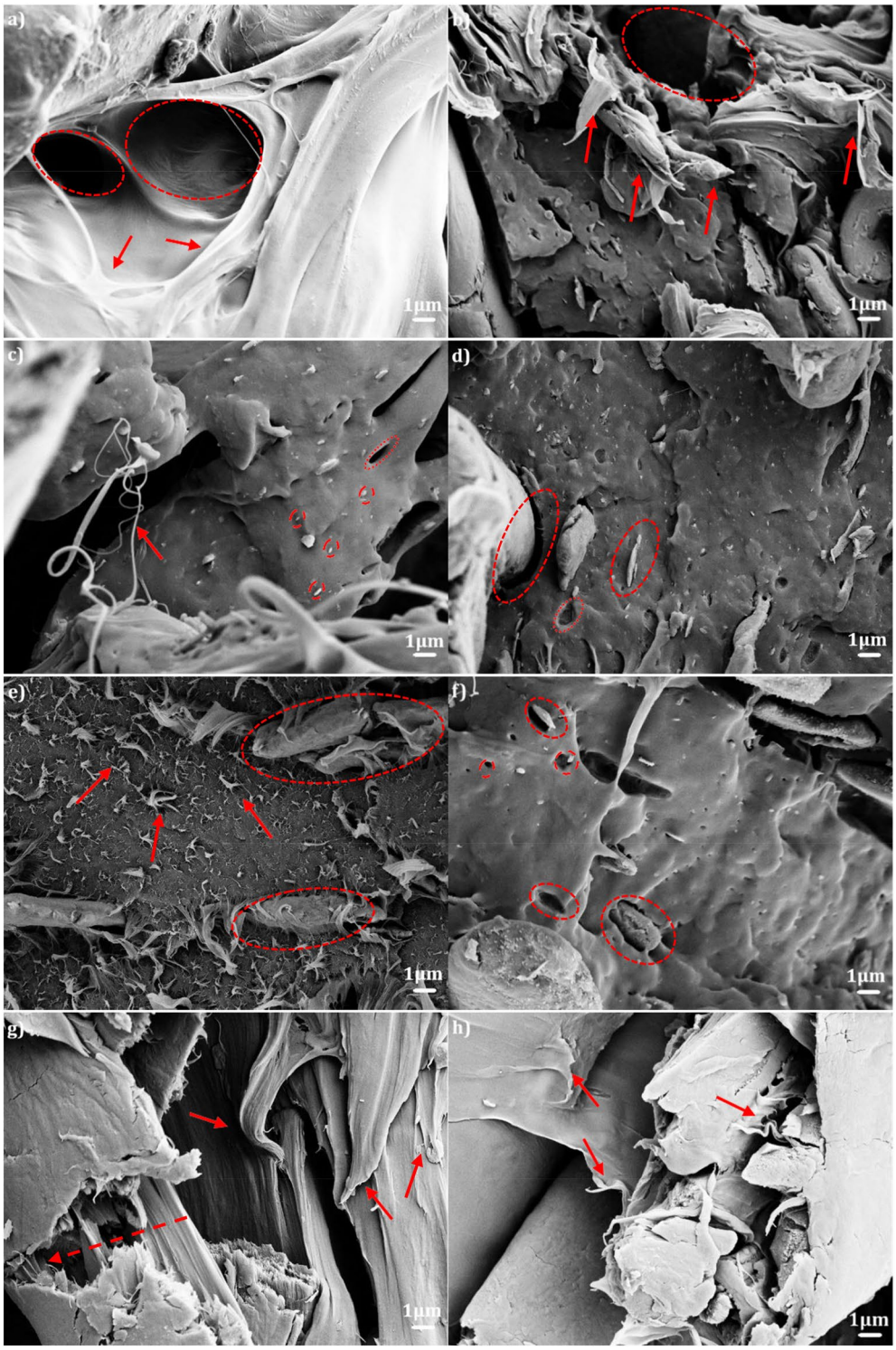

FIGURE 3 | FESEM micrographs of the specimens: (a) Neat PP (b) 70PP-30WF, and (c) 68PP-30WF-2HNT (d) 65PP-30WF-5HNT (e) 68PP-30WF-2RP53 (f) 68PP-30WF-2PY88TQ (g) 68PP-30WF-2 β-CD (h) 65PP-30WF-5 β-CD. [Color figure can be viewed at wileyonlinelibrary.com]

visually revealed with Figure 3f. The addition of 2 wt.% β-CD to WPC, as shown in Figure 3g, results in a uniform and smooth surface, offering the highest toughness among the WPC samples and preventing crack propagation in the wood fibers. Conversely, Figure 3h shows that increasing the β-CD content to 5 wt.% reduces the toughness of the WPC. Additionally, the inclusion of β-CD visibly improves the adhesion between PP and WF.

3.5 | Fourier-Transform Infrared (FTIR) Spectroscopy Analysis

The FT-IR spectra analysis results of WF and PP based WPC composites containing 2 wt.% and 5 wt.% HNT, β-CD, and 2 wt.% RP 53 and PY88TQ are presented in Figure 4. The broad absorption peak at 3350 cm^{-1} corresponds to the O – H stretching of

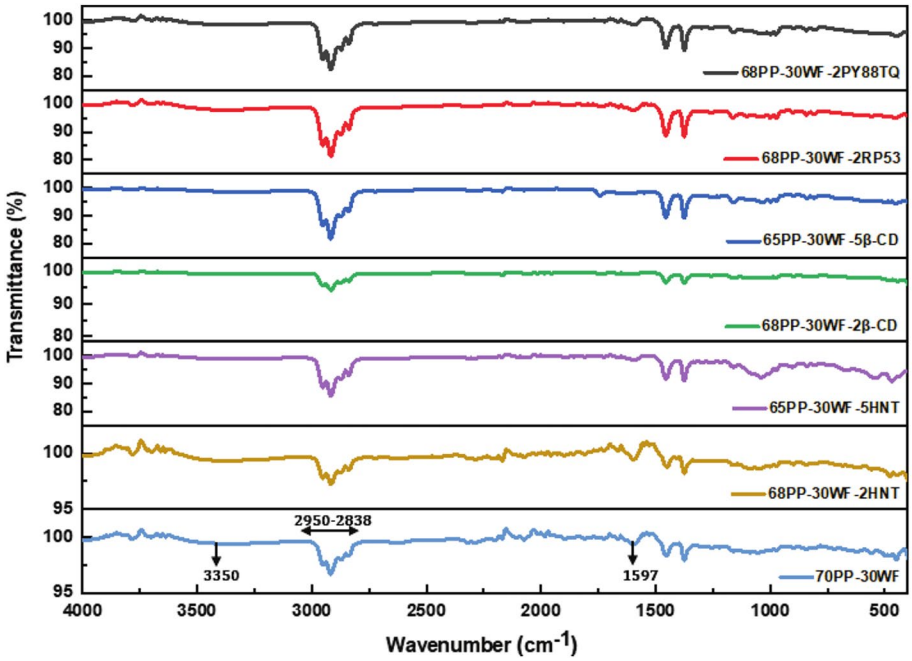

FIGURE 4 | FT-IR spectra of WPC samples composed of PP and 30 wt.% WF. [Color figure can be viewed at wileyonlinelibrary.com]

the alcoholic and phenolic hydroxyl groups in WPC belonging to WF. This broadening disappeared, especially with the addition of 5 wt.% HNT, due to the interaction of their free hydroxyl groups with those in WPC [47]. Additionally, this bonding causes the C-O ether peak at 1052 cm^{-1} to be more intense than the others. The interaction of 2 wt.% HNT and β-CD with WPC resulted in a decrease in the intensity of characteristic peaks of C-H methylene groups (symmetric and asymmetric) and the stretching vibration of the alkyl structure of the aliphatic group of PP at 2950, 2918, 2872, and 2838 cm^{-1}. The stretching vibrations of the aliphatic —C═C— bonds appear at 1597 cm^{-1}, with bond breakage spotted in WPC samples containing 2 wt.% and 5 wt.% β-CD and 5 wt.% HNT [48]. These results support the interaction of HNT and β-CD with WPCs and their influence on their structural properties.

3.6 | Thermal Analysis

The thermal stability of WPC with PP matrix was evaluated through TGA and DTG analyses, as shown in Figure 5, with the results provided in Table 4. All thermograms (weight change vs. temperature at the top and derivative of weight change vs. temperature at the bottom) which belong to WPCs in Figure 5 have similar trends. The thermal degradation of all WPCs was comprised of two stages. It is based on the fact that heterogeneity occurs in the polymer matrix in which the wood fiber is incorporated [38]. Results table and thermograms show that the first degradation observed in WPCs occurs at 361°C by 5 wt.% β-CD and HNT added WPC, which is close to the WPC without additive. While other additives have slightly higher degradation temperatures, the highest one belongs to the commercial additives and 2 wt.% HNT added WPCs with 364°C and 363°C. The ability of HNTs, which are relatively well-dispersed in the PP matrix, to trap VOCs occurring during thermal degradation

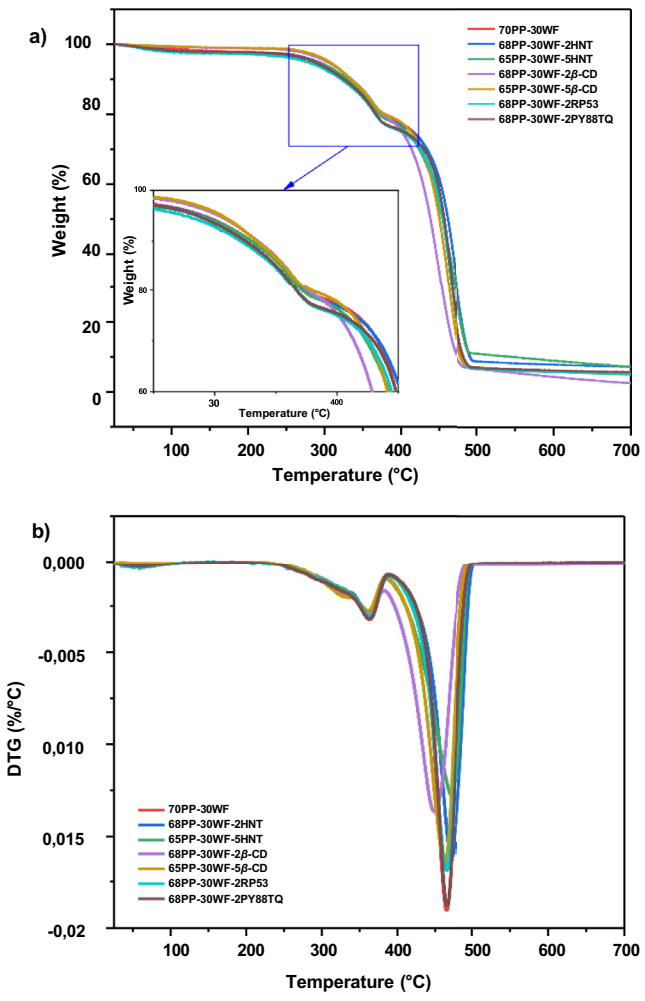

FIGURE 5 | TGA thermograms of all PP and 30 wt.% WF added WPC samples. [Color figure can be viewed at wileyonlinelibrary.com]

TABLE 4 | Degradation temperatures, weight loss, and % residue of WPCs.

	1st degradation		2nd degradation		
Sample Name	**Peak [°C]**	**Weight loss [%]**	**Peak [°C]**	**Weight loss [%]**	**Residue@ 700°C [%]**
70PP-30WF	361.0	21.9	465.0	72.4	5.6
70PP-30WF-2HNT	363.0	26.2	471.0	66.0	7.4
65PP-30WF-5HNT	361.0	21.5	472.0	70.8	7.5
68PP-30WF-2β-CD	362.0	19.7	449.0	76.4	2.7
65PP-30WF-5β-CD	361.0	21.3	463.0	73.4	5.3
68PP-30WF-2RP53	364.0	24.4	465.0	70.4	5.3
68PP-30WF-2PY88TQ	363.0	23.9	466.0	69.9	5.9

and limit polymer molecule mobility is responsible for the improved thermal stability [49, 50]. The same phenomenon was observed at the second decomposition stage. The curves in this stage, starting around 406°C, are not so similar as in the first step, with the highest weight loss which belongs to 2 wt.% β-CD added WPC [51]. However, the maximum peak decomposition temperature around 472°C was observed in the 2 and 5 wt.% HNT-containing WPC, which exhibited the lowest weight loss of WPC with 2 wt.% HNT, approximately 66% in this stage. The residue remaining at the end of the analysis was higher for HNT added WPCs due to the high thermal stability of HNT, which resulted in a higher degradation temperature. This phenomenon can be attributed to the high barrier effect of HNT that covers the surface and distributes heat and delays the combustion. Notably, as seen in Figure 5, HNT significantly reduces the rate of degradation.

The changes on the thermal transition temperatures of the specimens were examined by DSC analysis. The endothermic melting and exothermic crystallization thermograms obtained from DSC analysis are shown in Figure 6a,b below. In addition, melting temperature (Tm), cold crystallization temperature (Tc), melting enthalpy (ΔHm), cold crystallization enthalpy (ΔHc), and crystallinity (Xc) thermograms are given in Table 5. It was found that the melting temperature of PP increased after the 30 wt.% WF addition, indicating that the crystallization rate of WPC has accelerated. Following this, the temperature and degree of crystallization decreased with the addition of wood fiber content. The explanation for these declines is that wood fibers may hinder the flow of PP polymer and its molecular rearrangement, causing the crystallization process to be retarded. The addition of HNT to WPC led to an increase in melting temperature of about 1.5% and 7.5% of crystallization temperatures. Additionally, a decrease in crystallization degree of about 6% was observed due to interfacial interaction between HNT and PP [52]. This may be caused by silanol groups on the HNT surface hindering the movement of molecules in the PP polymer chain, preventing molecular packing [53]. Another explanation of this is that HNT causes polymer chains to crystallize more quickly when cooled. HNT functioned as a nucleation agent for PP, reducing the spherulite size and retarding PP crystal growth. Additionally, higher HNT loading (5 wt.% in WPC) yields aggregation in the PP matrix, and aggregated HNTs have lower nucleation capability due to reduced specific surface area, resulting in decreased

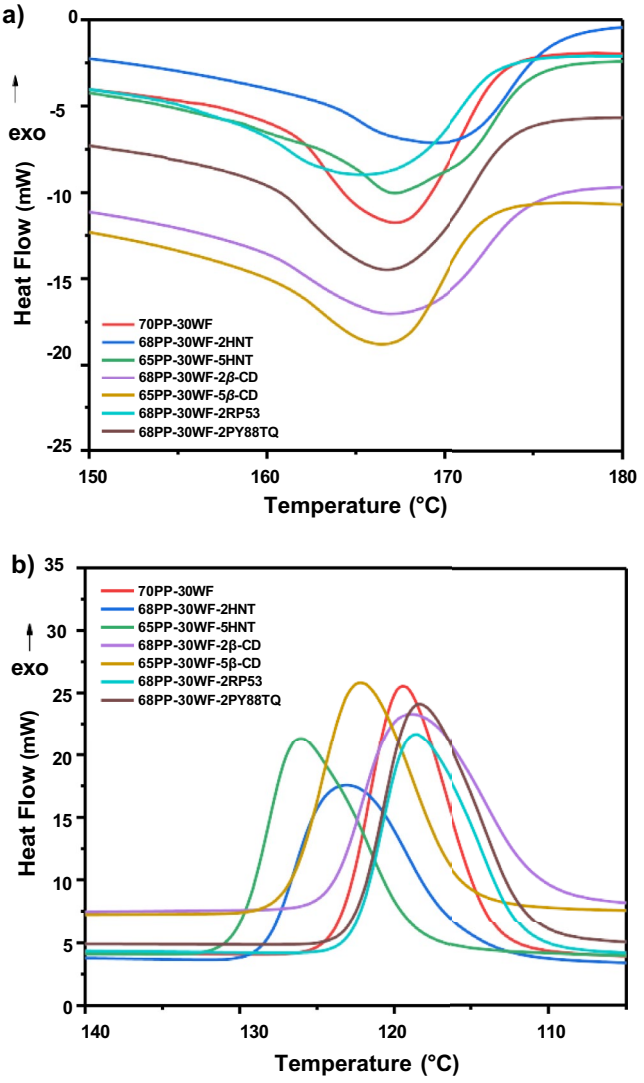

FIGURE 6 | DSC thermograms of PP and 30 wt.% WF added WPC, 2 and 5 wt.% HNT and β-CD added WPCs, and 2 wt.% RP 53 and PY88TQ added WPCs samples: (a) Melting peaks, (b) Crystallization peaks. [Color figure can be viewed at wileyonlinelibrary.com]

crystallinity [54]. The melting and crystallization temperatures in WPC are close to those of 2 wt.% RP53 and PY88TQ. However, PY88TQ has the highest degree of crystallization among other WPCs and is similar to Neat PP. This effect is the

TABLE 5 | DSC Summary of Tm, Tc, ΔHm, ΔHc, and Xc of the WPC with PP matrix samples.

Sample name	Tm [°C]	Tc [°C]	ΔHm [J/g]	ΔHc [J/g]	ΔHm° [J/g]	Xc [%]
70PP-30WF	166.7	120.4	74.1	71.6	207.0	51.1
70PP-30WF-2HNT	169.2	123.8	69.1	68.9	207.0	47.7
65PP-30WF-5HNT	166.8	130.2	69.7	68.6	207.0	48.1
68PP-30WF-2β-CD	166.1	119.8	73.8	73.6	207.0	50.9
65PP-30WF-5β-CD	165.7	123.1	71.9	70.5	207.0	49.6
68PP-30WF-2RP53	164.9	119.3	70.4	72.5	207.0	48.6
68PP-30WF-2PY88TQ	166.2	119.2	78.7	73.6	207.0	54.3

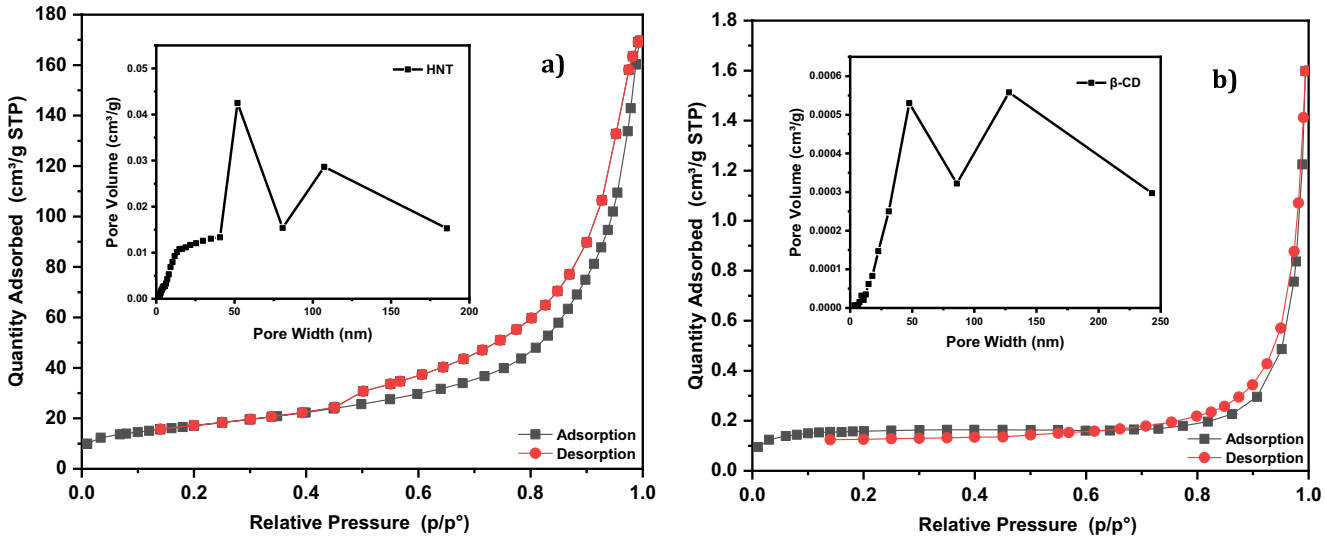

FIGURE 7 | BET adsorption–desorption isotherms and pore size distribution graphs for (a) HNTs and (b) β-CD. [Color figure can be viewed at wileyonlinelibrary.com]

TABLE 6 | Tabulated values (bottom) for surface area and pore volume for HNTs and β-CD.

Sample name	BET surface area [m^2/g]	Total pore volume [cm^3/g]	Average pore diameter [nm]
HNT	60.71	0.1622	10.69
β-CD	0.52	0.000737	5.65

inverse of using RP 53 in WPC. The addition of 2 and 5 wt.% β CD had no significant effect on the melting and crystallization temperature or degree of crystallinity in the WPC.

3.7 | BET Analysis

To better understand the adsorption behaviors of the HNTs and β-CD, the surface area and porosity characteristics of them were evaluated using nitrogen adsorption–desorption isotherms and Brunauer–Emmett–Teller (BET) analysis. The corresponding isotherms and pore size distributions are presented in Figure 7, and the key parameters are summarized in Table 6.

The distinct adsorption behaviors of HNTs and β-CD observed as VOC reduction in WPCs can be explained through their nitrogen adsorption–desorption isotherms and corresponding pore size distribution. BET analysis demonstrated the contrasting adsorption behaviors of HNT and β-CD. As shown in Figure 7a, the isotherm for HNTs displays a typical type IV behavior with a pronounced H3-type hysteresis loop, indicative of mesoporous structures [55]. The characteristics of surface area, total pore volume, and average pore diameter shown in Table 6 point to a surface area of 60.71 m^2/g and a mesoporous network (average pore size: 10.69 nm), favoring multilayer adsorption and VOC diffusion. The pore size distribution (in Figure 7a) reveals dominant mesopores around 10–15 nm, further confirming the material's capacity for accommodating relatively large VOC molecules and promoting physical adsorption through increased surface interactions [56]. In contrast, the adsorption–desorption isotherm of β-CD (Figure 7b) exhibits a much flatter profile with a very low total pore volume (0.000737 cm^3/g) and BET surface area (0.52 m^2/g), suggesting limited textural porosity. The average pore diameter, 5.65 nm, aligns with the expected dimensions of β-CD's toroidal molecular structure. The pore size distribution

(in Figure 7b) confirms a narrow range of mesopores with low volume, reinforcing its relatively low bulk adsorption capacity [57]. Despite these limitations, β-CD's effectiveness in targeting specific VOCs arises from its ability to form host–guest inclusion complexes through its hydrophobic cavity and hydrophilic exterior. This enables selective trapping of small polar VOCs, such as formaldehyde and aromatic compounds, and also benzaldehyde, as supported by GC–MS data [58–61]. Therefore, while HNTs primarily contribute through high-capacity, non-selective adsorption enabled by their large surface area and mesoporous network, β-CD offers selective molecular recognition. These complementary properties suggest their suitability for tailored WPC applications depending on whether bulk VOC reduction or targeted adsorption is prioritized.

4 | Conclusion

This study reveals that halloysite nanotubes (HNT) and β-cyclodextrin (β-CD) function as effective additives for enhancing the odor reduction, strength, and thermal resistance of wood plastic composites (WPCs) derived from polypropylene. HNT enabled this through considerable non-selective adsorption due to its mesoporous structure. β-CD, alternatively, efficiently trapped polar VOCs via host–guest inclusion complexation. Both sensory (jar) odor analysis and HS GC–MS tests showed that the formulation containing 5 wt.% HNT and 2 wt.% β-CD significantly reduced most of the VOC emissions, including 4-methyloctane, which is one of the key odorous compounds in WPCs with a polypropylene matrix.

The integration of HNT increased the material's strength and elasticity, whereas the addition of β-CD increased its toughness without compromising its total strength. Thermal and spectroscopic analyses shown that each addition is associated with the polypropylene matrix distinctly. The BET results confirmed their individual adsorption characteristics, illustrating their collaborative functionality in multiple uses.

The usage of each HNT and β-CD effectively produces WPCs that convey restricted odors while functioning successfully in indoor applications. In the future, the investigation of modifying the surfaces of HNT and β-CD will further improve their multifunctionality in composite systems.

Author Contributions

Gizem Kurtulmus: conceptualization (equal), investigation (lead), methodology (lead), resources (equal), validation (lead), writing – original draft (lead), writing – review and editing (lead). **Yusuf Ziya Menceloglu:** conceptualization (equal), investigation (supporting), methodology (supporting), project administration (lead), resources (supporting), supervision (lead), writing – original draft (supporting), writing – review and editing (supporting).

Acknowledgments

This study is supported by the Turkish Scientific and Technological Research Council of Türkiye (TÜBİTAK) and Kastamonu Entegre Wood Industry Co Inc. with Project Numbers 118C042 and 5230043.

Ethics Statement

The authors have nothing to report.

Conflicts of Interest

The authors declare no conflicts of interest.

Data Availability Statement

The data that support the findings of this study are available on request from the corresponding author. The data are not publicly available due to privacy or ethical restrictions.

References

1. Packaging Waste, "Environment," (2023), https://environment.ec.europa.eu/topics/waste-and-recycling/packaging-waste_en.

2. U.S. National Recycling Goal, "US EPA," (2023), https://www.epa.gov/circulareconomy/us-national-recycling-goal.

3. M. P. Wolcott and T. Adcock, "New Advances in Wood Fiber-Polymer Formulations," (2000) In: Proc Wood–Plastic Conference Plastics Technology Magazine and Polymer Process, Communications, 107–114.

4. K. Shelesh-Nezhad, H. Orang, and M. Motallebi, "The Effects of Adding Nano-Calcium Carbonate Particles on the Mechanical and Shrinkage Characteristics and Molding Process Consistency of PP/Nano-$CaCO_3$ Nanocomposites," (2012), https://doi.org/10.5772/35272.

5. S. Almaie, V. Vatanpour, M. H. Rasoulifard, and I. Koyuncu, "Volatile Organic Compounds (VOCs) Removal by Photocatalysts: A Review," *Chemosphere* 306 (2022): 135655, https://doi.org/10.1016/j.chemosphere.2022.135655.

6. S. V. Canevarolo, "Chain Scission Distribution Function for Polypropylene Degradation During Multiple Extrusions," *Polymer Degradation and Stability* 70, no. 1 (2000): 71–76, https://doi.org/10.1016/s0141-3910(00)00090-2.

7. P. Kang, P. Wu, Y. Jin, et al., "Formation and Emissions of Volatile Organic Compounds From Homo-PP and co-PP Resins During Manufacturing Process and Accelerated Photoaging Degradation," *Molecules* 25, no. 12 (2020): 2761, https://doi.org/10.3390/molecules25122761.

8. J. Fuller, D. White, H. Yi, J. Colley, Z. Vickery, and S. Liu, "Analysis of Volatile Compounds Causing Undesirable Odors in a Polypropylene-High-Density Polyethylene Recycled Plastic Resin With Solid-Phase Microextraction," *Chemosphere* 260 (2020): 127589, https://doi.org/10.1016/j.chemosphere.2020.127589.

9. T. Väisänen, K. Laitinen, L. Tomppo, et al., "A Rapid Technique for Monitoring Volatile Organic Compound Emissions From Wood–Plastic Composites," *Indoor and Built Environment* 27, no. 2 (2016): 194–204, https://doi.org/10.1177/1420326x16669976.

10. J. Ahn, S. K. Pandey, and K. Kim, "Comparison of GC-MS Calibration Properties of Volatile Organic Compounds and Relative Quantification Without Calibration Standards," *Journal of Chromatographic Science* 49, no. 1 (2011): 19–28, https://doi.org/10.1093/chrsci/49.1.19.

11. A. Behravesh, A. Z. Aghdam, and E. Soury, "Experimental Investigation of Injection Molding of Wood/Plastics Composites," *Journal of Reinforced Plastics and Composites* 29, no. 3 (2009): 456–465, https://doi.org/10.1177/0731684408099406.

12. S. Wang and A. Zhang, "Chemical Characterization of Smoke From the Production Process of Wood-Plastic Composites," *Forestry Studies in China* 9, no. 1 (2007): 57–62, https://doi.org/10.1007/s11632-007-0010-6.

13. E. Garofalo, L. Taurino, L. Di Maio, H. C. Neitzert, and L. Incarnato, "Assessment of Melt Compounding With Zeolites as an Effective Deodorization Strategy for Mixed Plastic Wastes and Comparison With

Degassing," *Polymers* 15, no. 8 (2023): 1858, https://doi.org/10.3390/polym15081858.

14. X. Zhang, B. Gao, A. E. Creamer, C. Cao, and Y. Li, "Adsorption of VOCs Onto Engineered Carbon Materials: A Review," *Journal of Hazardous Materials* 338 (2017): 102–123, https://doi.org/10.1016/j.jhazmat.2017.05.013.

15. W. Zou, B. Gao, Y. S. Ok, and L. Dong, "Integrated Adsorption and Photocatalytic Degradation of Volatile Organic Compounds (VOCs) Using Carbon-Based Nanocomposites: A Critical Review," *Chemosphere* 218 (2018): 845–859, https://doi.org/10.1016/j.chemosphere.2018.11.175.

16. A. M. Da Silva, "Room at the Top as Well as at the Bottom: Structure of Functional Food Inclusion Compounds," in *InTech eBooks* (InTech, 2018), https://doi.org/10.5772/intechopen.74162.

17. W. Zhao, B. Shi, and C. Hu, "Adsorption Properties of β-Cyclodextrin for Adsorbing Aromatic Hydrocarbons From the Gas Phase and Water," *Journal of Macromolecular Science Part B* 47, no. 1 (2007): 211–216, https://doi.org/10.1080/00222340701748792.

18. P. Yuan, D. Tan, and F. Annabi-Bergaya, "Properties and Applications of Halloysite Nanotubes: Recent Research Advances and Future Prospects," *Applied Clay Science* 112 (2015): 75–93, https://doi.org/10.1016/j.clay.2015.05.001.

19. L. W. Wong, C. B. S. Goh, P. Pasbakhsh, and J. B. L. Tan, "Natural Hollow Clay Nanotubes and Their Applications as Polymer Nanocomposites in Tissue Engineering," *Journal of Science: Advanced Materials and Devices* 7, no. 2 (2022): 100431, https://doi.org/10.1016/j.jsamd.2022.100431.

20. M. Fahimizadeh, L. W. Wong, Z. Baifa, et al., "Halloysite Clay Nanotubes: Innovative Applications by Smart Systems," *Applied Clay Science* 251 (2024): 107319, https://doi.org/10.1016/j.clay.2024.107319.

21. O. Kotova, S. Sun, E. Kotova, A. Ponariaydov, and R. Brodskaya, "Aluminosilicates: Interphase Boundary Interactions and Nature Engineering of Nanostructures," *Journal of Physics: Conference Series* 2315, no. 1 (2022): 012003, https://doi.org/10.1088/1742-6596/2315/1/012003.

22. M. P. Kapoor, M. Moriwaki, K. Minoura, D. Timm, A. Abe, and K. Kito, "Structural Investigation of Hesperetin-7-O-Glucoside Inclusion Complex With β-Cyclodextrin: A Spectroscopic Assessment," *Molecules* 27, no. 17 (2022): 5395, https://doi.org/10.3390/molecules27175395.

23. A. Singh, V. Krishna, A. Angerhofer, B. Do, G. MacDonald, and B. Moudgil, "Copper Coated Silica Nanoparticles for Odor Removal," *Langmuir* 26, no. 20 (2010): 15837–15844, https://doi.org/10.1021/la100793u.

24. K. Ramadass, C. I. Sathish, S. MariaRuban, et al., "Carbon Nanoflakes and Nanotubes From Halloysite Nanoclays and Their Superior Performance in CO2 Capture and Energy Storage," *ACS Applied Materials & Interfaces* 12, no. 10 (2020): 11922–11933, https://doi.org/10.1021/acsami.9b21510.

25. C. E. Y. Erpek, G. Ozkoc, and U. Yilmazer, "Comparison of Natural Halloysite With Synthetic Carbon Nanotubes in Poly(Lactic Acid) Based Composites," *Polymer Composites* 38, no. 11 (2015): 2337–2346, https://doi.org/10.1002/pc.23816.

26. A. Garg, S. Basu, R. L. Mahajan, and R. Mehta, "Enhancement in Mechanical Properties of GFRP-Coal-Derived Graphene Oxide Composites by Addition of Multiwalled Carbon Nanotubes and Halloysite Nanotubes: A Comparative Study," *Polymer Composites* 45 (2024): 13164–13179, https://doi.org/10.1002/pc.28694.

27. T. Guo, R. Zhang, X. Wang, et al., "Porous Structure of B-Cyclodextrin for CO2 Capture: Structural Remodeling by Thermal Activation," *Molecules* 27, no. 21 (2022): 7375, https://doi.org/10.3390/molecules27217375.

28. V. Kadam, Y. B. Truong, C. Easton, et al., "Electrospun Polyacrylonitrile/B-Cyclodextrin Composite Membranes for Simultaneous Air Filtration and Adsorption of Volatile Organic Compounds," *ACS Applied Nano Materials* 1, no. 8 (2018): 4268–4277, https://doi.org/10.1021/acsanm.8b01056.

29. V. Kadam, Y. B. Truong, J. Schutz, I. L. Kyratzis, R. Padhye, and L. Wang, "Gelatin/β–Cyclodextrin Bio–Nanofibers as Respiratory Filter Media for Filtration of Aerosols and Volatile Organic Compounds at Low Air Resistance," *Journal of Hazardous Materials* 403 (2020): 123841, https://doi.org/10.1016/j.jhazmat.2020.123841.

30. S. Jana, S. Das, C. Ghosh, A. Maity, and M. Pradhan, "Halloysite Nanotubes Capturing Isotope Selective Atmospheric CO2," *Scientific Reports* 5, no. 1 (2015): 8711, https://doi.org/10.1038/srep08711.

31. V. S. Wadi, K. K. Jena, K. Halique, and S. M. Alhassan, "Enhanced Mechanical Toughness of Isotactic Polypropylene Using Bulk Molybdenum Disulfide," *ACS Omega* 5, no. 20 (2020): 11394–11401, https://doi.org/10.1021/acsomega.0c00419.

32. X. Gao, Q. Li, W. Cheng, G. Han, and L. Xuan, "Optimization of High Temperature and Pressurized Steam Modified Wood Fibers for High-Density Polyethylene Matrix Composites Using the Orthogonal Design Method," *Materials* 9, no. 10 (2016): 847, https://doi.org/10.3390/ma9100847.

33. X. Duan, C. Yuan, Q. Guo, S. Niu, K. He, and G. Xia, "Preparation of Halloysite Nanotubes-Encapsulated Magnetic Microspheres for Elemental Mercury Removal From Coal-Fired Flue Gas," *Journal of Hazardous Materials* 406 (2020): 124683, https://doi.org/10.1016/j.jhazmat.2020.124683.

34. L. Yu, K. Dean, and L. Li, "Polymer Blends and Composites From Renewable Resources," *Progress in Polymer Science* 31, no. 6 (2006): 576–602, https://doi.org/10.1016/j.progpolymsci.2006.03.002.

35. T. Lomonaco, E. Manco, A. Corti, et al., "Release of Harmful Volatile Organic Compounds (VOCs) From Photo-Degraded Plastic Debris: A Neglected Source of Environmental Pollution," *Journal of Hazardous Materials* 394 (2020): 122596, https://doi.org/10.1016/j.jhazmat.2020.122596.

36. K. S. Prado, M. Strangl, S. R. Pereira, et al., "Odor Characterization of Post-Consumer and Recycled Automotive Polypropylene by Different Sensory Evaluation Methods and Instrumental Analysis," *Waste Management* 115 (2020): 36–46, https://doi.org/10.1016/j.wasman.2020.07.021.

37. S. Zeng, Y. Zeng, P. Guo, C. Hu, and Z. Wang, "Characterization of Odors and Volatile Organic Compounds Changes to Recycled High-Density Polyethylene Through Mechanical Recycling," *Polymer Degradation and Stability* 208 (2023): 110263, https://doi.org/10.1016/j.polymdegradstab.2023.110263.

38. T. Adamová, J. Hradecký, and M. Pánek, "Volatile Organic Compounds (VOCs) From Wood and Wood-Based Panels: Methods for Evaluation, Potential Health Risks, and Mitigation," *Polymers* 12, no. 10 (2020): 2289, https://doi.org/10.3390/polym12102289.

39. N. Sallem-Idrissi, C. Vanderghem, T. Pacary, et al., "Lignin Degradation and Stability: Volatile Organic Compounds (VOCs) Analysis Throughout Processing," *Polymer Degradation and Stability* 130 (2016): 30–37, https://doi.org/10.1016/j.polymdegradstab.2016.05.028.

40. Y. Li, H. Chen, and Y. Wang, "Efficient Removal of VOCs Using Mesoporous Nanomaterials," *Journal of Hazardous Materials* 381 (2020): 120998, https://doi.org/10.1016/j.jhazmat.2019.

41. J. H. Kim, J. S. Lee, and D. S. Lee, "Inclusion Complexation of VOCs by β-Cyclodextrin," *Industrial & Engineering Chemistry Research* 58, no. 1 (2019): 135–142, https://doi.org/10.1021/acs.iecr.8b04715.

42. P. Krishnaiah, S. Manickam, C. T. Ratnam, P. Raghu, S. P. Kumar, and B. Jeon, "Mechanical, Thermal and Dynamic-Mechanical Studies of Functionalized Halloysite Nanotubes Reinforced Polypropylene Composites," *Polymers and Polymer Composites* 29, no. 8 (2020): 1212–1221, https://doi.org/10.1177/0967391120965115.

43. E. Tekay, "Halloysit Nanotüp Takviyeli Kopoliester Termoplastik Elastomer Kompozitler: Isıl ve Mekanik Ozelliklerin Incelenmesi," *El-Cezeri Fen Ve Mühendislik Dergisi* 7, no. 3 (2020): 1343–1354, https://doi.org/10.31202/ecjse.764528.

44. P. V. Joseph, K. Joseph, and S. Thomas, "Effect of Processing Variables on the Mechanical Properties of Sisal-Fiber-Reinforced Polypropylene Composites," *Composites Science and Technology* 59, no. 11 (1999): 1625–1640, https://doi.org/10.1023/A:1014704223702.

45. Y. Li and H. Shimizu, "Improvement in Toughness of Polypropylene by Melt Compounding With Nanoscale Silica Particles," *Polymer* 50 (2009): 4669–4679, https://doi.org/10.1016/j.polymer.2009.07.024.

46. N. M. Stark and R. E. Rowlands, "Effects of Wood Fiber Characteristics on Mechanical Properties of Wood/Polypropylene Composites," *Wood and Fiber Science* 35, no. 2 (2003): 167–174.

47. K. Lee and Y. Chang, "Thermal, Mechanical, and Rheological Properties of Poly(ε-Caprolactone)/halloysite Nanotube Nanocomposites," *Journal of Applied Polymer Science* 128, no. 5 (2012): 2807–2816, https://doi.org/10.1002/app.38457.

48. A. K. Mohanty, M. Misra, and L. T. Drzal, "Sustainable Bio-Composites From Renewable Resources: Opportunities and Challenges in the Green Materials World," *Journal of Polymers and the Environment* 10 (2002): 19–26, https://doi.org/10.1023/A:1021013921916.

49. J. Guo, Y. Tang, and Z. Xu, "Performance and Thermal Behavior of Wood Plastic Composite Produced by Nonmetals of Pulverized Waste Printed Circuit Boards," *Journal of Hazardous Materials* 179, no. 1–3 (2010): 203–207, https://doi.org/10.1016/j.jhazmat.2010.02.080.

50. B. Wang and H. Huang, "Effects of Halloysite Nanotube Orientation on Crystallization and Thermal Stability of Polypropylene Nanocomposites," *Polymer Degradation and Stability* 98, no. 9 (2013): 1601–1608, https://doi.org/10.1016/j.polymdegradstab.2013.06.022.

51. E. Esmizadeh, C. Tzoganakis, and T. H. Mekonnen, "Degradation Behavior of Polypropylene During Reprocessing and Its Biocomposites: Thermal and Oxidative Degradation Kinetics," *Polymers* 12, no. 8 (2020): 1627, https://doi.org/10.3390/polym12081627.

52. X. Li, D. Tan, L. Xie, et al., "Effect of Surface Property of Halloysite on the Crystallization Behavior of PBAT," *Applied Clay Science* 157 (2018): 218–226, https://doi.org/10.1016/j.clay.2018.02.005.

53. H. C. Bidsorkhi, H. Adelnia, R. H. Pour, and M. Soheilmoghaddam, "Preparation and Characterization of Ethylene-Vinyl Acetate/Halloysite Nanotube Nanocomposites," *Journal of Materials Science* 50, no. 8 (2015): 3237–3245, https://doi.org/10.1007/s10853-015-8891-6.

54. M. Liu, B. Guo, M. Du, F. Chen, and D. Jia, "Halloysite Nanotubes as a Novel β-Nucleating Agent for Isotactic Polypropylene," *Polymer* 50, no. 13 (2009): 3022–3030, https://doi.org/10.1016/j.polymer.2009.04.052.

55. M. Thommes, K. Kaneko, A. V. Neimark, et al., "Physisorption of Gases, With Special Reference to the Evaluation of Surface Area and Pore Size Distribution (IUPAC Technical Report)," *Pure and Applied Chemistry* 87, no. 9–10 (2015): 1051–1069, https://doi.org/10.1515/pac-2014-1117.

56. Y. M. Lvov and E. Abdullayev, "Functional Polymer–Clay Nanotube Composites With Sustained Release of Chemical Agents," *Progress in Polymer Science* 38, no. 10–11 (2013): 1690–1719, https://doi.org/10.1016/j.progpolymsci.2013.05.009.

57. T. Loftsson and D. Duchêne, "Cyclodextrins and Their Pharmaceutical Applications," *International Journal of Pharmaceutics* 329, no. 1–2 (2007): 1–11, https://doi.org/10.1016/j.ijpharm.2006.10.044.

58. J. You, Y. Teng, B. Zhang, and Z. Fang, "Electrospun Nanofiber Membranes of β-Cyclodextrin for VOC Removal: Adsorption Performance and Mechanisms," *Separation and Purification Technology* 259 (2021): 118145, https://doi.org/10.1016/j.seppur.2020.118145.

59. G. Crini, "Recent Developments in Polysaccharide-Based Materials Used as Adsorbents in Wastewater Treatment," *Progress in Polymer Science* 30, no. 1 (2005): 38–70, https://doi.org/10.1016/j.progpolymsci.2004.11.002.

60. H. Li, Q. Ma, and J. Wu, "Removal of Formaldehyde by β-Cyclodextrin Based Electrospun Nanofibers," *Environmental Science: Nano* 7 (2020): 341–349, https://doi.org/10.1039/C9EN00900J.

61. W. Saenger, "Cyclodextrin Inclusion Compounds in Research and Industry," *Angewandte Chemie International Edition* 19, no. 5 (1980): 344–362, https://doi.org/10.1002/anie.198003441.